Accident Analysis and Prevention 111 (2018) 328–337

Contents lists available at ScienceDirect

Accident Analysis and Prevention

journal homepage: www.elsevier.com/locate/aap

Safety assessment on pedestrian crossing environments using MLS data

Mario Soilán[a,*], Belén Riveiro[a], Ana Sánchez-Rodríguez[b], Pedro Arias[b]

[a] Department of Materials Engineering, Applied Mechanics and Construction, School of Industrial Engineering, University of Vigo, 36310, Spain
[b] Department of Natural Resources and Environmental Engineering, School of Mining Engineering, University of Vigo, 36310, Vigo, Spain

ARTICLE INFO

Keywords:
Mobile laser scanning
Point cloud processing
Safety assessment
Classification
Geographic information system

ABSTRACT

In the framework of infrastructure analysis and maintenance in an urban environment, it is important to address the safety of every road user. This paper presents a methodology for the evaluation of several safety indicators on pedestrian crossing environments using geometric and radiometric information extracted from 3D point clouds collected by a Mobile Mapping System (MMS). The methodology is divided in four main modules which analyze the accessibility of the crossing area, the presence of traffic lights and traffic signs, and the visibility between a driver and a pedestrian on the proximities of a pedestrian crossing. The outputs of the analysis are exported to a Geographic Information System (GIS) where they are visualized and can be further processed in the context of city management. The methodology has been tested on approximately 30 pedestrian crossings in cluttered urban environments of two different cities. Results show that MMS are a valid mean to assess the safety of a specific urban environment, regarding its geometric conditions. Remarkable results are presented on traffic light classification, with a global F-score close to 95%.

1. Introduction

The assessment and improvement of traffic safety is essential for the development of contemporary and humanized cities. According to the European Road Safety Observatory (ERSO), more than 5000 pedestrians were killed in road accidents in the EU in 2014, being that a 21% of all road fatalities (ERSO, 2016). The most common cause of road fatality involving pedestrians are run overs in urban areas. In 2013, run overs were the cause of 50% of the fatal accidents in urban areas in Spain (AXA, 2014). Moreover, more than 3500 people were injured on run over accidents, being contusions and bone fractures the most common consequences. However, run overs are easy to prevent to a certain extent (Fundación Mutua Madrileña, 2013). Most of the run over accidents happen in pedestrian crossing areas, being the driver the main responsible of the accident. There exists an extensive literature regarding characteristics and behavioral analysis of run over accidents as well as measures to take in order to prevent these accidents (Hamed, 2001; Jiménez-Mejías et al., 2016; Retting et al., 2003; US Department of Transportation, 2001; Várhelyi, 1998). In order to assess the safety of the road environment, different models have been developed: Lassarre et al. (2007) measure the accident risk based on the exposure of a pedestrian at a certain location on an urban area; Kelly et al. (2007) assess the walkability of pedestrian environments by identifying and weighting parameters such as the quality of the pavement, the traffic volume or the street lightning. Basile et al. (2010) develop a safety index for the assessment of the safety on pedestrian crossing environments which is based on four main criteria: Spatial and temporal design, day-time visibility, night-time visibility and accessibility.

All the mentioned safety assessments are conducted manually, based on on-site inspections and surveys. Nowadays, LiDAR based mobile mapping technology is able to collect 3D data in a reliable, accurate manner (Puente et al. 2013a,b) and allows for the automatic or semi-automatic collection of geometric and semantic parameters in road environments, hence avoiding the manual collection of a large proportion of the required assessment data. The literature regarding the acquisition of data that may be used for safety assessments is vast. Works as (Miyazaki et al., 2014; Zhou and Vosselman, 2012) are focused on the detection of curbs in 3D data acquired with laser scanner. Serna and Marcotegui (2013) propose an accessibility analysis once the curbs are detected, establishing itineraries for people in wheelchairs according to the obstacles found in the road. In addition to being detected, several urban objects with an impact on road safety assessment can be semantically classified in order to get a better understanding of a 3D scene. For example, in Refs. Serna and Marcotegui (2014) and Yang et al. (2015) objects such as buildings, vehicles, trees or poles are classified from cluttered urban 3D scenes. Recently, Yang et al. (2017) proposed a semantic labelling framework of 3D point clouds based on appending several features on different scales of previously segmented objects. Combining point-based features such as Fast Point Feature Histogram (FPFH), segment-based features (principal directions, sizes

* Corresponding author.
E-mail address: msoilan@uvigo.es (M. Soilán).

https://doi.org/10.1016/j.aap.2017.12.009
Received 21 August 2017; Received in revised form 22 November 2017; Accepted 11 December 2017
Available online 20 December 2017
0001-4575/ © 2017 Elsevier Ltd. All rights reserved.

and dimensionality of each segmented object), object-based features (viewpoint feature histogram) and contextual features, a classification model was developed to distinguish objects such as traffic signs, guardrails or power lines among others. Research is also focused on the classification of road network assets, such as vertical signage (Riveiro et al., 2015; Wen et al., 2015) and road markings (Cheng et al., 2017; Guan et al., 2014), with promising results for both elements. Yu et al. (2016) are able to detect and classify traffic signage with state of the art accuracies using bag-of-visual-phrases representations for the detection task and a deep Boltzmann machine feature encoder for the classification task, where features are directly extracted from 2D images where the detected 3D traffic signs have been previously projected. Similarly (Yu et al., 2015a) propose a method for the extraction and classification of road markings consisting of a segmentation process which relies on an intensity-based multisegment thresholding, and a classification based on heuristic decisions for large-size markings and a deep learning model that takes binary representations of the road markings as feature.

Regarding visibility analysis, there exist research that study the effects of different hazards that may deteriorate the visibility conditions (Abdel-Aty et al., 2011; Mueller and Trick, 2012), but there is little research analyzing visibility parameters from dense 3D point clouds. A relevant work is the one presented by Alsadik et al. (2014) where they address three different problems related with visibility: Camera network design, guidance with synthetic images and gap detection in a point cloud; based on surface triangulation and voxel-based approaches.

In this work, a methodology that assists the safety assessment on pedestrian crossing environments taking advantage of mobile mapping technology is proposed. The motivation for this work is to close the gap that exists between the manual safety assessment analyses that are carried out to this day and the capabilities of mobile mapping technology to offer an accurate description of road environments in an automated way. The contributions of this work are therefore (1) The definition of a workflow that extracts geometric and semantic information from a 3D point cloud which can be utilized to define the safety of a pedestrian crossing environment; and (2) The organized visualization, as a safety map, of all the data on a Geographic Information System (GIS).

2. Methodology

The proposed methodology is organized in four modules, each of them aiming to collect geometric and semantic information on the environment of a pedestrian crossing: (1) Accessibility analysis, (2) Traffic lights classification, (3) Traffic signs classification, and (4) Visibility analysis. Data defining pedestrian crossings are considered as an input for this work as obtained from (Soilán et al., 2017). The methodology workflow is shown in Fig. 1.

2.1. Point cloud preprocessing

Let $\{\boldsymbol{P},\ \boldsymbol{t},\ \mathcal{M}\}$ be the inputs for this work, where $\boldsymbol{P} = \{\boldsymbol{x},\ \boldsymbol{y},\ \boldsymbol{z},\ \boldsymbol{I},\ \boldsymbol{t_s}\}$ is a point cloud containing the $(x,\ y,\ z)$ coordinates together with intensity and time stamp for each 3D point, $\boldsymbol{t} = \{\boldsymbol{x_t},\ \boldsymbol{y_t},\ \boldsymbol{z_t},\ \boldsymbol{t_{st}}\}$ represents the trajectory of the vehicle as collected by its navigation system, and $\mathcal{M} = \{M_1,\ ...,M_i,\ ...,M_n\},\ i = 1...n\,|\,M_i \subset \boldsymbol{P}$ contains the set of pedestrian crossing objects that have been detected within $\boldsymbol{P}$ applying (Soilán et al., 2017) methodology, which consists of a number of processing steps that, given a point cloud $\boldsymbol{P}$, selects 3D points belonging to road markings by taking advantage of the reflective properties of the paint material, and subsequently classifies them (distinguishing several types of arrows and pedestrian crossings), finally allowing to extract each pedestrian crossing as a subset of $\boldsymbol{P}$.

First, the input point cloud $\boldsymbol{P}$ is preprocessed. This work intends to study the environment of the pedestrian crossings in the point cloud, therefore a large proportion of the 3D points will not provide relevant information and can be removed from further processing steps. For that purpose, a transformation matrix $\boldsymbol{T}$ is obtained for each pedestrian crossing in $\mathcal{M}$ such that

$$\boldsymbol{T} = \begin{matrix} \boldsymbol{R}_{3x3} & \boldsymbol{t}_{3x1} \\ 0_{1x3} & 1 \end{matrix} \tag{1}$$

where $\boldsymbol{R}_{3x3}$ represents a rotation around z-axis of an angle α_z formed between the y-axis and the longitudinal direction of the road marking, and $\boldsymbol{t}_{3x1}$ represents a translation equal to the centroid of the pedestrian crossing coordinates.

Using the matrix $\boldsymbol{T}$, the input 3D data get centered on a pedestrian crossing, and orientated towards its principal direction (Eq. 2).

$$\boldsymbol{P_{Th}} = \boldsymbol{T}\cdot\boldsymbol{P_h} \tag{2}$$

where $\boldsymbol{P_{Th}}$ contains the homogeneous coordinates of the transformed point cloud and $\boldsymbol{P_h}$ the original homogeneous coordinates. Let $\boldsymbol{P_T}$ be the transformed point cloud removing the homogeneous notation.

The second preprocessing step consists of the definition of the pedestrian crossing environment. Using the transformed point cloud $\boldsymbol{P_T}$, it is straightforward to select those points that define the surroundings of the crossing area. Indices $\boldsymbol{i_s}$ of points whose y coordinate is between $(l/2 - 5)m$ and $(l/2 + 5)m$, where l is the length of the pedestrian crossing along y axis, are selected. Let $S(\boldsymbol{P},\ \boldsymbol{i})$ be a function that selects a subset of points with indices $\boldsymbol{i}$ within a point cloud $\boldsymbol{P}$. The environment of the pedestrian crossing is defined as $\boldsymbol{P_s} = S(\boldsymbol{P_T},\ \boldsymbol{i_s})$

Finally, ground and non-ground points are segmented on point cloud $\boldsymbol{P_s}$. For this purpose, a voxel-based segmentation inspired on (Douillard et al., 2011) algorithm for dense data is applied. The point cloud is voxelized, that is, a cubic cell grid is defined. Then, for every voxel, vertical mean and variance are computed and subsequently a region growing algorithm groups neighboring voxels whose mean and variance differences are less than two respective thresholds, d_μ and d_σ. In order to speed up this process, voxels that contain points from the pedestrian crossing are selected as seeds for the region growing algorithm, and the ground segment is defined with the grouped voxels once the growing process finishes. The algorithm returns the indices of the points in $\boldsymbol{P_T}$ and $\boldsymbol{P}$ (both point clouds share the same indices) that belong to the ground and non-ground segments, $\boldsymbol{i_g},\ \boldsymbol{i_{ng}}$, defining ground and non-ground point clouds as $\boldsymbol{P_g} = S(\boldsymbol{P_s},\ \boldsymbol{i_g})$ and $\boldsymbol{P_{ng}} = S(\boldsymbol{P_s},\ \boldsymbol{i_{ng}})$ respectively.

2.2. Accessibility analysis

The Spanish Ministry of Public Works and Transport has defined the maximum transversal and longitudinal slope on accessible pedestrian routes as 2% and 8% respectively. Furthermore, the maximum slope on accessible ramps has been set as 12% (Ministerio de Fomento, 2010). These specifications ensure an accessible and safe route for disabled people, and therefore they are essential for the quality of the crossing environment. In this section, accessibility at the entrances of a pedestrian crossing is studied. First, it is necessary to detect non-accessible areas on the ground segment. Normally, urban areas intended for circulation of vehicles and pedestrians are separated by curbs, small steps forming an edge between the road and the sidewalk. An accessible pedestrian route cannot include curbs, therefore the presence or absence of this obstacle has to be detected in the crossing area.

Given the geometric information in the 3D point cloud $\boldsymbol{P_s}$, curbs are detected following a modification of Wang et al. (2015) road boundary detection algorithm, consisting on a saliency analysis which separates the input point cloud in two segments, one of them containing points that belong to horizontal surfaces, and other with the remaining points (including façades, walls or curbs). Salient points are grouped via Euclidean clustering (Yu et al., 2015b) and filtered based on their elevation, horizontal length and distance to the trajectory (Wang et al., 2015), obtaining a set of point indices $\boldsymbol{i_c}$ that represent potential curbs. Finally, false detections are avoided intersecting indices $\boldsymbol{i_c}$ and $\boldsymbol{i_g}$, such

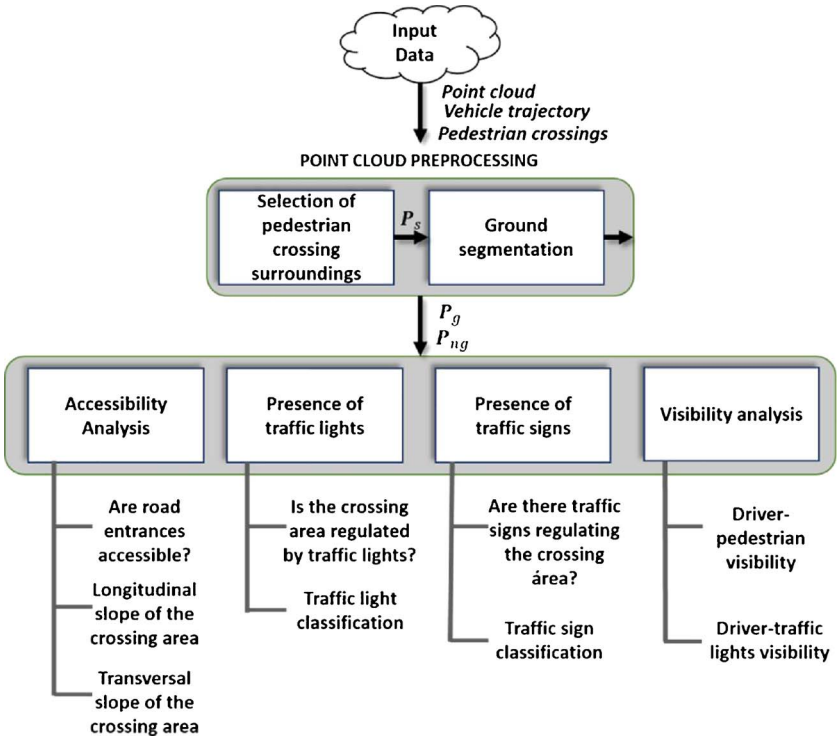

Fig. 1. Methodology workflow.

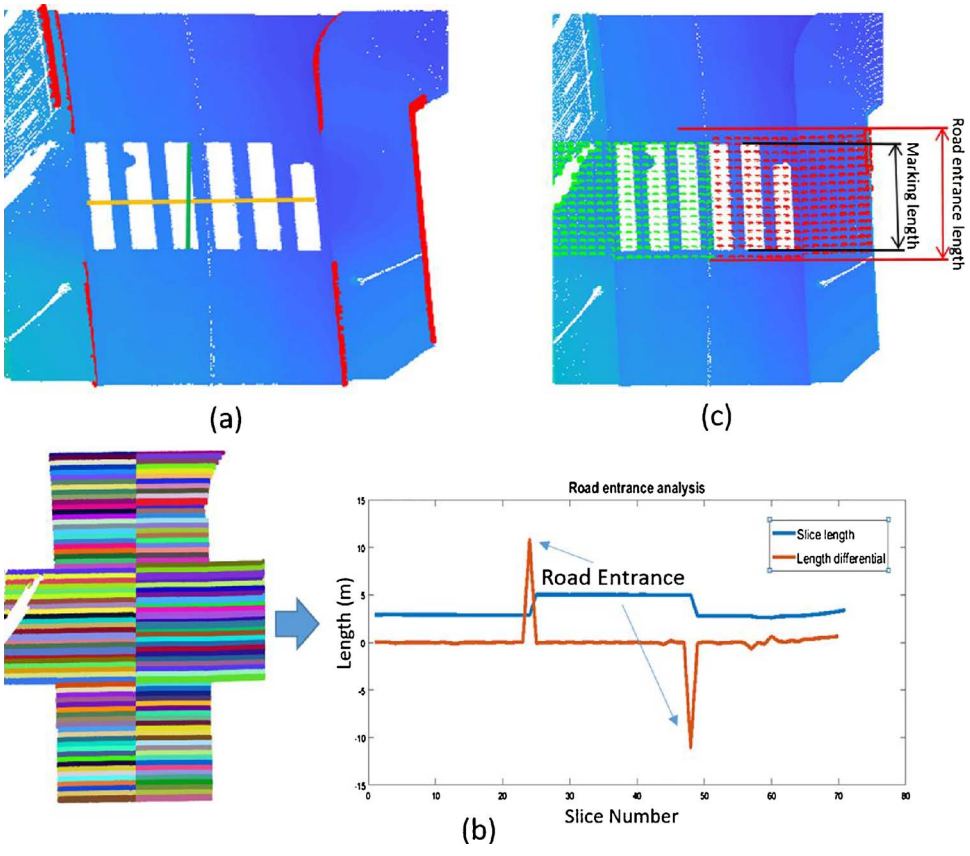

Fig. 2. Accessibility analysis. (a) The curb map $\boldsymbol{P}_{curbs}$ is highlighted in red, defining non-accessible areas. Green and orange lines are used to define longitudinal and transversal slopes respectively. (b) The point cloud is divided in slices on the right and the left sides of the pedestrian crossing. Each slice grows until a point from the curb map is found. By comparing the length of neighbouring slices, it is possible to define road entrances. (c) The accessibility is evaluated by checking the overlap between the road marking and the road entrance (dotted areas).

that a curb map $\boldsymbol{P}_{curbs} = S(\boldsymbol{P}_s,\ (\boldsymbol{i}_c \cap \boldsymbol{i}_g))$ is defined (Fig. 2a).

Then, $\boldsymbol{P}_g$ is divided in a number of slices along x-axis (perpendicular to the trajectory direction) and a region growing process is performed on each slice following:

1) Slice generation: $\boldsymbol{s}_i = (x_i,\ y_i,\ z_i) \subset \boldsymbol{P}_g \mid y_i \rangle\ min_y + (i-1)\cdot s_{slice},\ y_i \leq min_y + i \cdot s_{slice}$, where min_y is the minimum value of the y coordinate in $\boldsymbol{P}_g$ and s_{slice} is the width of each slice, which was set to 20 cm.
2) Two different seed points are selected: $s_{left_i} = (x,\ y,\ z) \subset \boldsymbol{S}_i \mid x = \min(\boldsymbol{x} \in S_i \mid x \rangle 0)$, and $s_{right_i} = (x,\ y,\ z) \subset \boldsymbol{S}_i \mid x = \max(\boldsymbol{x} \in S_i \mid x < 0)$.

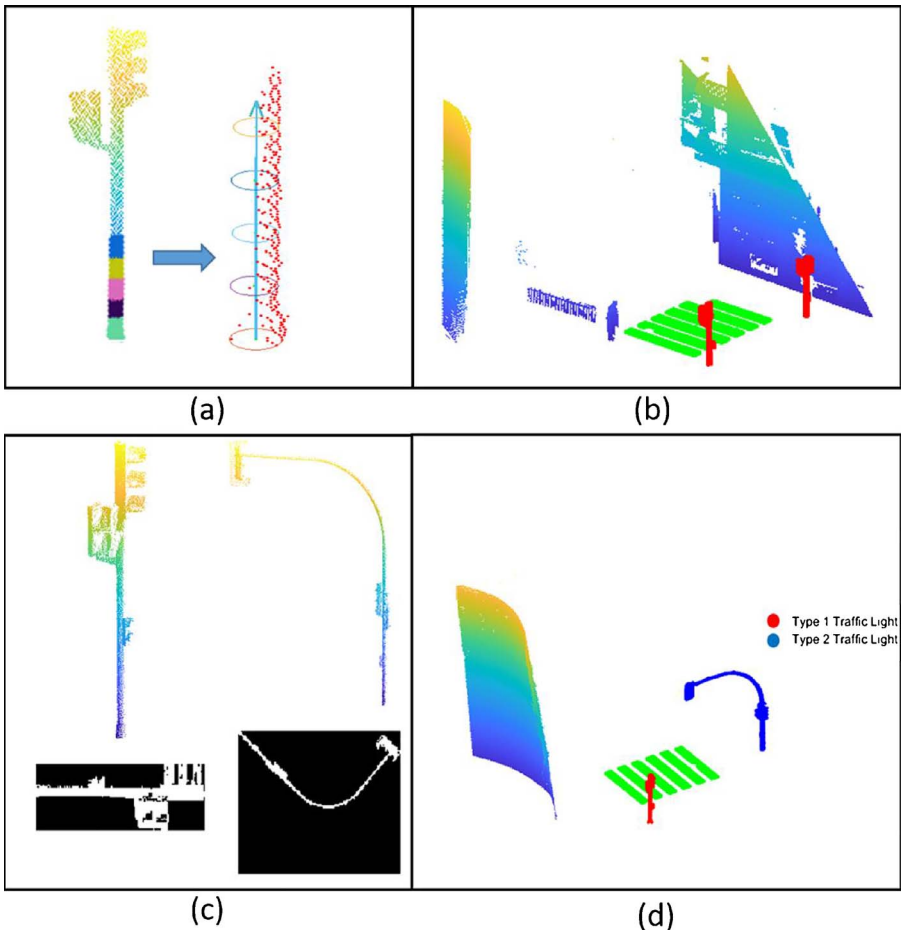

Fig. 3. Presence of traffic lights. (a) Pole-like objects segmentation. Circles are fit to a group of horizontal profiles. The quality of the circle adjustment, the position of the centers and the radius of the circles are used for defining the object as a pole. (b) Pole-like objects are segmented from the point cloud $\boldsymbol{P}_{ng}$. (c) Each pole-like object is projected to a 2D plane and binary images are created, where features for classification are extracted. (d) Two types of traffic lights are classified.

3) For each seed, points of the slice are grouped independently on right and left side of the pedestrian crossing area. The region growing stops whenever a point of the curb map $\boldsymbol{P}_{curbs}$ is found.

After this process, accessible road entrances are determined by comparing the length of neighboring slides, as depicted in Fig. 2b.

Finally, the coordinates of the detected road entrances and the pedestrian crossing are matched. If the intersection between y coordinates of both elements leads to an interval of 2 meters or more (Fig. 2c), the pedestrian crossing is classified as accessible (note that the accessibility is studied separately on the right and on the left); otherwise, it is classified as non-accessible crossing. According to Ministerio de Fomento (2010), the width of the road entrance should be between 1.2 and 1.8 meters depending on the regional normative, therefore the accessibility output complies with national standards.

Other relevant parameters that can be extracted from this analysis are the longitudinal and transversal slopes of the pedestrian crossing area. Given the 3D point cloud data of a pedestrian crossing marking M_i, the slopes can be obtained as

$$transversal\ slope\ (\%) = \frac{abs(z(x_{max}) - z(x_{min}))}{x_{max} - x_{min}} \cdot 100 \quad (3)$$

$$longitudinal\ slope\ (\%) = \frac{abs(z(y_{max}) - z(y_{min}))}{y_{max} - y_{min}} \cdot 100 \quad (4)$$

where x_{max}, x_{min} are the x coordinates of two points of the road marking which form a line that approximates the trajectory of a pedestrian who is crossing the road, $z(x_{max})$, $z(x_{\min})$ are the heights of these points, and analogously, y_{max}, y_{min} are the y coordinates of two points forming a line which is perpendicular to the aforementioned trajectory (Fig. 2a).

This processing module outputs the following information for each pedestrian crossing in $\mathcal{M}$:

1) *Access_left (Boolean)*: Indicates whether the pedestrian crossing area on the left side of the trajectory direction is part of an accessible pedestrian route.
2) *Access_right* (*Boolean*): Indicates whether the pedestrian crossing area on the right side of the trajectory direction is part of an accessible pedestrian route.
3) *Longitudinal_slope:* Numerical value of the longitudinal slope as obtained in Eq. 3. National standards define the maximum longitudinal slope as 8%.
4) *Transversal_slope*: Numerical value of the transversal slope as obtained in Eq. 4. National standards define the maximum transversal slope as 2%.

2.3. Presence of traffic lights

This processing module defines whether or not a pedestrian crossing area is controlled by traffic lights. Geometrically, traffic lights can be defined as pole-like objects with standard measures that are typically located close to the edge of the road. Aiming for detecting these objects, point cloud $\boldsymbol{P}_{ng}$ is analyzed for each pedestrian crossing in $\mathcal{M}$. It contains all the non-ground 3D points on the pedestrian crossing surroundings. First, a Euclidean clustering process groups 3D points together, obtaining a set of clusters $C = \{C_1, ...,C_i, ...,C_n\} \,|\, C_i \subset \boldsymbol{P}_{ng}$. Subsequently, a segmentation process filters out those clusters that do not contain a pole-like object. Finally, a supervised classification approach distinguishes traffic lights from other pole-like objects as trees or street lights.

2.3.1. Pole-like object segmentation

For each cluster C_i, the point with minimum elevation $\min_h$ is obtained. Then, a distance $d_t = 0.2m$ is defined and a group of horizontal profiles is defined such that profile number k contains points with z coordinates within $\min_h + d_t(k-1)$ and $\min_h + d_t \cdot k$. Then, the 3D points of each horizontal profile are projected on a horizontal plane $Z = \min_h + d_t(k-1)$ and a circle is fitted from the resulting coordinates. For each circle, its radius , center $\boldsymbol{O}_k$, and mean-squared error with respect to the points of the profile, MSE_k are computed, and the following parameters are retrieved for each cluster C_i (Fig. 3a):

1) Maximum radius $\max(r_k) | k = 1...n$.
2) Angle α between the principal direction of the 3D points that correspond with the circle centers $\boldsymbol{O}_k | k = 1...n$ (which is obtained applying a Principal Component Analysis (PCA) and selecting the eigenvector corresponding to the largest eigenvalue) and the vertical [0 0 1].
3) Average value of mean-squared errors $\overline{MSE} = \sum_{k=1}^{n} \frac{MSE_k}{n}$.
4) Height of the cluster, h_i.

The cluster C_i will be considered a pole-like object if:

$$\begin{cases} \alpha < 10^o \\ max(r_k) < 2m \\ \overline{MSE} < 0.001 \\ h_i < 10m \end{cases}$$

where radius and height thresholds have been set according to the standard sizes of traffic lights, while angle and mean-squared error thresholds have been set empirically in order to avoid as many false positives as possible while avoiding false negatives.

Clusters that do not satisfy these conditions are filtered out, and only pole-like clusters $C_p = \{C_{p1}...C_{pi}...C_{pn}\} | C_p \subset C$ are fed into the classification step (Fig. 3b).

2.3.2. Traffic light classification

Traffic lights are found via supervised classification. Specifically, two different models have been computed for classifying the main types of traffic light in Europe: Column traffic lights (Type 1) and mast arm traffic lights (Type 2). First, for each pole-like cluster, PCA is applied and the points on the cluster are transformed to the coordinate system of the three principal directions. Then, transformed points are projected into a 2D raster grid with a variable grid size such that the number of columns is fixed to 128 for every point cluster. Subsequently a binary image is computed from the raster grid, setting to true pixels corresponding to cells that contain at least one point (Fig. 3c).

Binary images $\mathcal{I} = \{\boldsymbol{I}_1,...,\boldsymbol{I}_i, ...,\boldsymbol{I}_n\}$ are divided in two sets according to the image aspect ratio (number of columns / number of rows). Studying the standard dimensions of traffic lights, it was considered that images with an aspect ratio larger than 3 would contain all Type 1 traffic lights, while the remaining images contain all Type 2 traffic lights. Image sets can be defined as $\mathcal{I}_{\boldsymbol{b}} = \boldsymbol{I_i} \in \mathcal{I} | aspect\ ratio(\boldsymbol{I}_i) \geq 3$, $\mathcal{I}_{\boldsymbol{s}} = \boldsymbol{I_i} \in \mathcal{I} | aspect\ ratio(\boldsymbol{I}_i) < 3$.

Images from sets $\mathcal{I}_{\boldsymbol{s}}$ and $\mathcal{I}_{\boldsymbol{b}}$ are resized to [42 128] and [96 128] sizes respectively. If the original image is bigger than the resized version, it is resized using bicubic interpolation. Otherwise, it is padded with zeros. With this step, it is possible to extract image-based features of fixed size for the classification stage.

For the classification of Type 1 traffic lights, a pixel distribution feature is defined. For each resized image from $\mathcal{I}_{\boldsymbol{b}}$, the proportions of '1' pixels on each row and each column are computed and subsequently appended, obtaining a feature of 170 elements. The model used for the classification of the features is a Cubic SVM.

Regarding Type 2 traffic lights, the binary image is directly transformed into a feature, appending all its pixel values to a single vector. The binary feature has 12,288 elements and it is classified using a two layer feed forward neural network with sigmoid hidden and softmax output neurons.

Model training details for both classification models can be found in Section 3. This processing module outputs a subset of C_p which contains only those 3D point clusters classified as traffic lights of Type 1 or 2 (Fig. 3d).

2.4. Presence of traffic signs

Vertical signage is an essential element of the infrastructure. It regulates traffic and warns drivers of potential road hazards. In the context of a pedestrian crossing environment, traffic signs may inform a driver of the presence of traffic lights or an area with pedestrian priority, diminishing the probability of run overs. Previous work (Soilán et al., 2016) posed a vertical traffic sign detection and classification algorithm, based on the radiometric properties of the traffic sign panels (González-Jorge et al., 2013) which are related with the intensity property of the 3D point cloud. Traffic sign panels are detected by selecting clusters of points with large intensity values, and filtering out clusters whose size and dimensionality do not correspond with standard sizes for traffic signs.

Then, in order to give a semantic description of the detected traffic signs, their symbols have to be interpreted. However, the resolution of the 3D point cloud is not enough to recognize it, therefore RGB imagery provided by the MMS has to be used. Given the calibration parameters of the MMS cameras (Puente et al., 2013b), a cluster of 3D points can be projected onto images where it can be seen. Traffic sign recognition is carried out using the Deep Neural Network model from (Arcos-García et al., 2017), which comprises convolutional and spatial transformer layers, and show state-of-the-art performance.

This processing module outputs a set of traffic sign objects containing geometrical parameters (position, azimuth of the traffic sign panel or distance to the trajectory, among others) and semantic information (traffic sign class).

2.5. Visibility analysis

It is important to ensure the visibility between drivers and pedestrians in pedestrian crossing environments. In order to avoid run overs, pedestrians are encouraged to cross the road only in places with good visibility, and administrations are advised to remove any obstacles (street furniture, parking spaces, vegetation) that prevent a good visibility (RACE; Goodyear, 2015).

According to the Spanish department responsible for the transport network (Directorate General of Traffic (DGT)), any object is considered to be in the visible area of a driver when being the vehicle located at the minimum distance needed for it to stop in safe conditions (stopping distance), the object is within the vision field of the driver and there is not any obstacle occluding the visual contact. With the available 3D point cloud data, it is possible to check if a pedestrian would be visible for a driver on a certain location.

First, the stopping distance (S_d) has to be computed. It is defined as:

$$S_d = \frac{V}{3.6} \cdot t_{pr} + \frac{V^2}{254(\mu_r \pm i)} \quad (5)$$

where V is the vehicle speed, measured in km/h, t_{pr} is the reaction time, μ_r is the friction coefficient (whose values are tabulated, depending on the speed) between wheels and pavement, and i is the slope of the road.

Aiming for a conservative study of the visibility, the values selected for both V and t_{pr} are 50 km/h (maximum allowed speed in urban areas) and 2 s respectively. Under these assumptions, the stopping distance of a vehicle is approximately 35 m for a flat surface.

Let $M_i \in \mathcal{M}$ be a pedestrian crossing object and $\boldsymbol{P}_{ng}$ be its corresponding non-ground point cloud. In order to check the pedestrian-

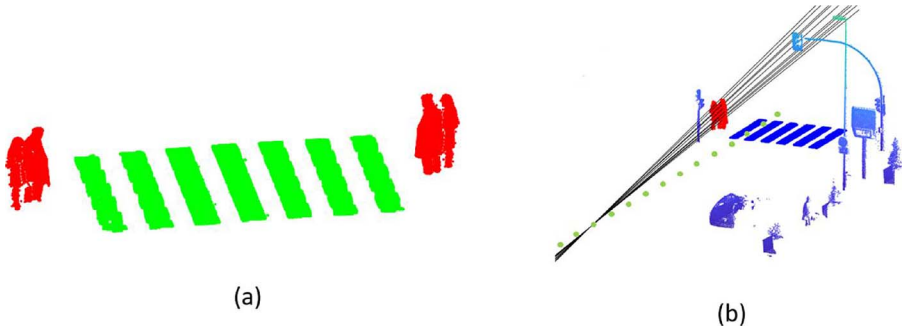

Fig. 4. Visibility analysis. (a) A pedestrian template is located at both sides of the pedestrian crossing in order to check the visibility from the perspective of a driver. (b) A set of lines of sight is defined between each point of view and each point of the pedestrian template. For each line, obstacles may be detected as points inside spheres centered on different points within each line of sight.

vehicle visibility, a 3D point cloud pedestrian template is merged with $\boldsymbol{P}_{ng}$ at both sides of the pedestrian crossing. Note that the coordinates had been transformed such that x-axis and y-axis represent the transversal and longitudinal directions of the pedestrian crossing (Section 2.1). Therefore, the integration of the template within $\boldsymbol{P}_{ng}$ is straightforward: Being (x_{tp}, y_{tp}, z_{tp}) the point with minimum elevation of the template, a translation vector is defined such that $\boldsymbol{t}_{tp} = (x_{tp} - (a - 1),\ y_{tp} - b,\ z_{tp} - c)$ where a is the minimum x coordinate, b is the average y coordinate and c is the minimum z coordinate of the pedestrian crossing 3D points. This translation locates the template on the left side of the pedestrian crossing. A rotation of 180 degrees about the origin locates the template on the right side, allowing the visibility analysis on both sides of the crossing area (Fig. 4a).

The visibility analysis relies on González-Jorge et al. (2016) vision model, based on a ray-tracing algorithm which creates a Line of Sight (LoS) from the driver point of view to a target point, and checks for occlusions that may be caused by obstacles such as cars, walls or trees. Occlusions are detected as points within a 3D cylinder of diameter 0.5m created along the LoS.

For the visibility between the driver and a pedestrian who is nearby a pedestrian crossing, a set of driver points of view (PoV) is created, using the trajectory points between the stopping distance and the pedestrian crossing and defining the eyes of the driver 1.2 meters above the ground.

A visibility definition is given for each PoV such that it is labelled as 1) Point with good visibility, 2) Point with bad visibility, or 3) Point with no visibility. The labelling procedure is as follows: First, a LoS is created between the PoV $(x_o,\ y_o,\ z_o)$ and each point $(x_p,\ y_p,\ z_p)$ of the pedestrian template, obtaining a set of parametric equations

$$\begin{aligned} x &= x_o + t\cdot(x_p - x_o) \\ y &= y_o + t\cdot(y_p - y_o) \\ z &= z_o + t\cdot(z_p - z_o) \end{aligned} \tag{6}$$

The angle α_v between the LoS segment, whose director vector is $(x_p - x_o),\ (y_p - y_o),\ (z_p - z_o)\|$ and the direction of the trajectory is computed in order to check whether or not the pedestrian is on the horizontal field of view (FoV) of the driver. This range depends on the vehicle speed, narrowing as the vehicle moves faster (tunnel vision). Considering a driver with an average eyesight, the horizontal field of view when driving at 50 km/h is slightly less than 90° (FoV = 45° on each side). If $\alpha_v > FoV$ for any LoS, the point of view is labelled as a point with no visibility.

If the pedestrian is located within the horizontal field of view of the driver, the existence of occlusions is examined. They are found as a number of 3D points within a volume around a LoS. For each line, a number of points equally spaced and belonging to the line are selected by varying the parameter t from Eq. (6) (Fig. 4b). Each point will be the center of a sphere of diameter $d_{sph} = 0.25m$. An occlusion is found whenever a number n_p of points of $\boldsymbol{P}_{ng}$ lies within one of the spheres for the selected LoS. For the results seen in Section 4, t was given values from 0.01 to 1 in steps of 0.01, generating 100 points per line; while n_p, considering the typical point cloud density for the study case dataset (Section 3) has been set to 50 points, therefore selecting as occlusion points spherical volumes whose densities are larger than ${}^{np}/_{V_{sph}} = 765\ {}^{pts}/_{m^3}$. Having in account the point cloud density and the distance from the laser scanner to the possible occlusions, these parameters ensure that occlusion points do not belong to scattered or noisy points.

Finally, each PoV is labelled according to the following criteria, based on the proportion of visible points of the pedestrian from the perspective of the driver:

1) *Point of view with good visibility*: More than 75% of the pedestrian points are visible. Small objects such as bins, benches or other urban furniture may slightly affect the visibility of small parts of the crossing area without affecting the visual contact between driver and pedestrian.
2) *Point with bad visibility*: Between 25 and 75% of the pedestrian points are visible. Parked cars, trees or trash cans may impede the visibility of the pedestrian, increasing the hazard level on the pedestrian crossing.
3) *Point with no visibility*: Less than a 25% of the pedestrian points are visible. The visibility is critical for these points.

Furthermore, the same process can be applied in order to analyze the visibility of the detected traffic lights. If one or more traffic lights are detected applying the method on Section 2.3, the visibility of the point cluster that defines the traffic light from the stopping distance is checked. The same labelling approach assigns a visibility label to each traffic light.

This processing module outputs the set of points of view used for analyzing the visibility together with the visibility label for each point of view, for driver-pedestrian visibility and driver-traffic lights visibility.

2.6. Data exportation and visualization

All the data obtained in Sections 2.2–2.5 is gathered in order to be visualized, or further processed, in a GIS software:

- *Accesibility*: The accessibility on both sides of the pedestrian crossing is defined in Section 2.2 as a Boolean variable, set to true if the crossing area is accessible. In order to clarify which variable corresponds to the left side and the right side of the pedestrian crossing within a GIS layer (notice that left and right are conceptually defined given the trajectory direction), a point from each side of the pedestrian crossing is associated to the corresponding accessibility variable. Furthermore, slopes are integrated as a property of the pedestrian crossing object.
- *Traffic Lights:* Those traffic lights that are classified as Type 1 are exported as the 2D centroid of the (x, y) coordinates of the object. Differently, Type 2 traffic lights are exported as a 2D bounding box resulting from the projection of their points on the XY plane. A

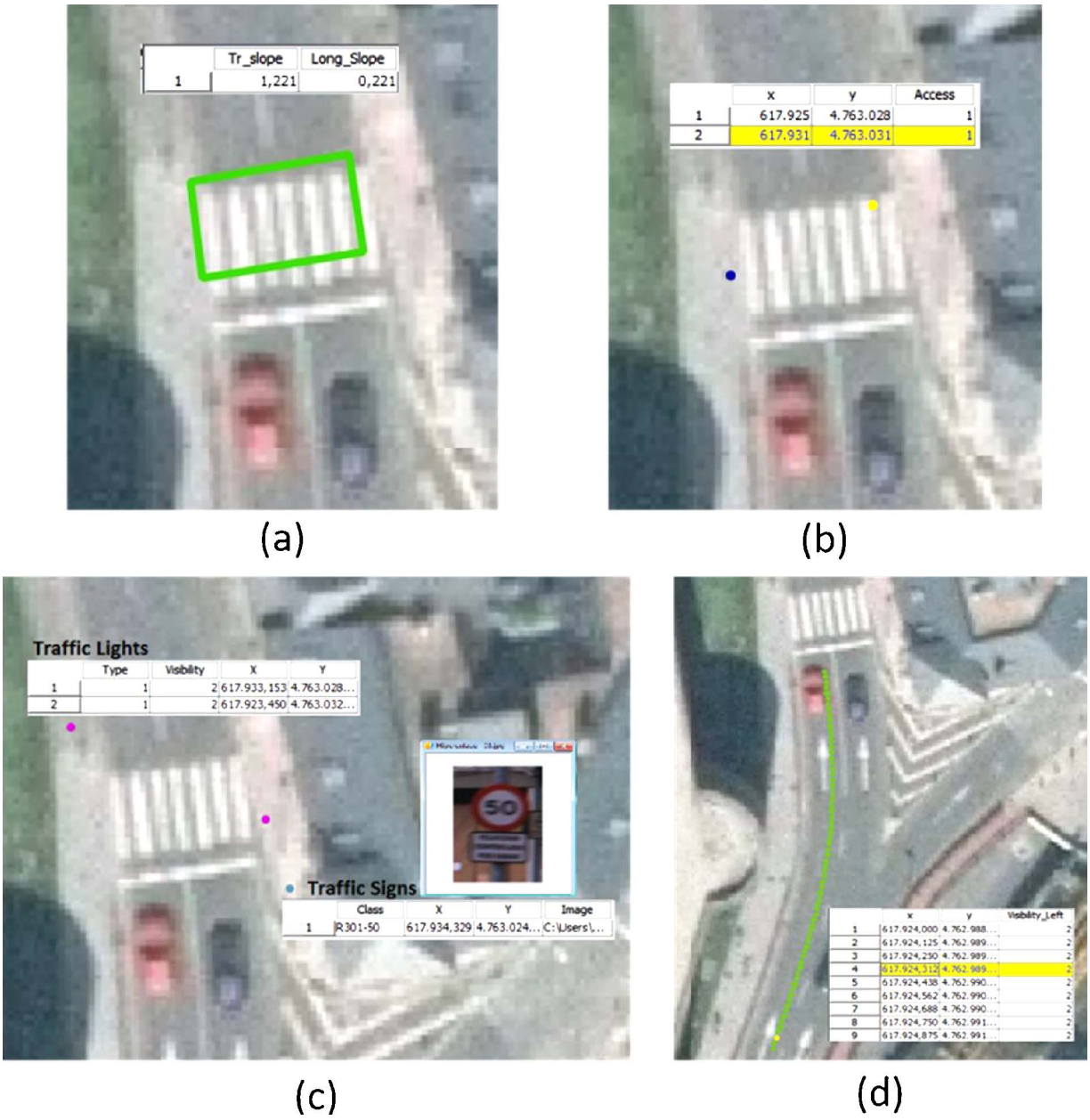

Fig. 5. Visualization of the output data. (a) The pedestrian crossing is defined with a bounding box and the transversal and longitudinal slope. (b) The accessibility is defined with two points, one on each side of the crossing area, each of them having a binary variable attached indicating whether the crossing area is part of an accessible route or not. (c) Traffic lights and traffic signs are defined with their 2D coordinates, a visibility label, and a class obtained during the classification process. Traffic signs may have an image attached if the MMS collects 2D imagery. (d) The driver-pedestrian visibility is defined as a group of 2D points from the stopping distance with a visibility label attached to them.

visibility label is also related to each traffic light.

- *Traffic Signs:* Each traffic sign is represented in a GIS layer as a 2D point with several properties such as the class of the sign. Furthermore, a 2D image of the traffic sign can be attached to each point in the layer whenever imagery is available on the MMS data.
- *Visibility:* It is represented as a group of 2D points corresponding with the projections on the XY plane of the analyzed points of view, each of them associated to a visibility label indicating the visibility degree from the vehicle stopping distance to the pedestrian crossing.

The visualization of these data is exemplified in Fig. 5. A total of six GIS layers can be visualized superimposed over a georreferenced ortophoto. The road marking is visualized as a rectangular bounding box with the slopes as properties (Fig. 5a). The accessibility (Fig. 5b), traffic lights, traffic signs (Fig. 5c) and visibility (Fig. 5d) are shown as 2D points with several attributes attached to them.

Finally, a safety rating can be computed for each pedestrian crossing using all the gathered data. There are different possible approaches in order to quantify the safety of an urban area. Basile et al. (2010) weight a large number of parameters, some of which are based on the geometry (pedestrian crossing width, accessibility, presence of obstacles, presence of traffic lights, etc.) but also non-geometrical parameters (efficiency and duration of red-green traffic light phases, audible signals, etc.). Similarly, (RACE, 2009) took part in a pedestrian crossing safety analysis across 22 European countries, establishing four thematic blocks that have an impact on the quality of a pedestrian crossing: Crossing system, day-time visibility, night-time visibility, and accessibility. Weighting all these parameters is under a subjective criteria up to the road authorities.

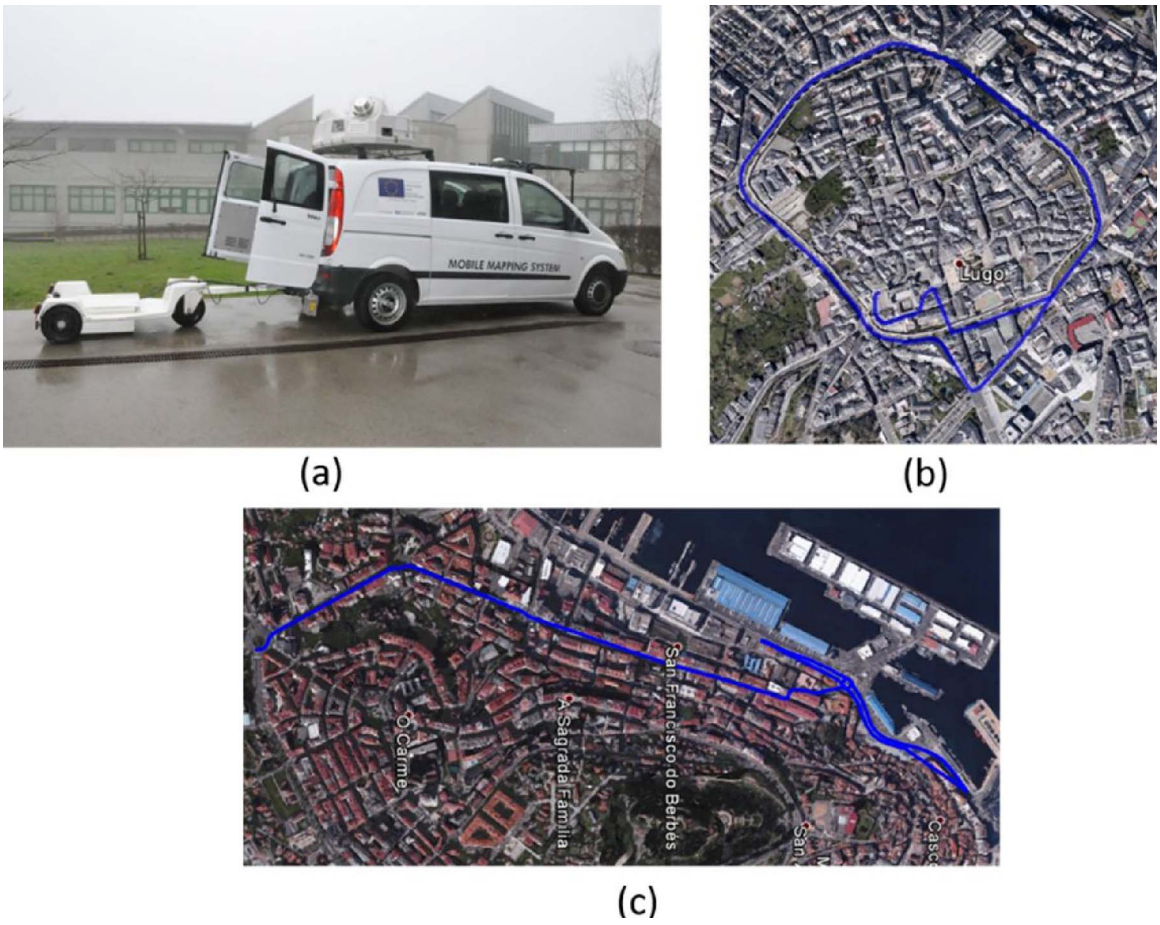

Fig. 6. Case study. (a) Mobile Mapping System used on the survey. (b) Lugo (city center) trajectory data. (c) Vigo (School zone) trajectory data.

3. Case study

The LYNX Mobile Mapper by Optech (Fig. 6a) was used for the collection of the data. It has two LiDAR sensor heads with a field of view of 360°, which collects up to 500,000 measurements per second. The sensor heads were placed with an angle of 45° with respect to the trajectory and 90° between their rotational axes. The navigation system comprises an Inertial Measurement Unit (IMU) and a two-antenna heading measurement system (GAMS). More technical specifications can be found in (Puente et al., 2013b).

The methodology in Section 2 was tested in two different scenarios in the northwest of Spain. The first one, located in the city of Lugo, is a cluttered one-way avenue surrounding the city center (Fig. 6b). The second scenario is a two-way street in a school zone in the city of Vigo (Fig. 6c). Furthermore, the classification models used in Section 2.3 were trained with 3D data from two large avenues in Vigo. The point clouds were segmented in order to find pole-like structures following Section 2.3.1 method. A label was manually assigned to each pole-like object, defining five classes: Traffic light (Type 1), traffic light (Type 2), street lamp, tree, and other pole-like objects. Table 1 summarizes the case study relevant data. A total of 27 pedestrian crossing areas have been studied and the classification data contains almost 800 objects among the five classes.

Table 1
Case study data.

Area	Usage	Points	Relevant info
Lugo (City center)	Methodology testing	97 762 746	15 pedestrian crossings
Vigo (School zone)	Methodology testing	52 779 090	12 pedestrian crossings
Vigo (Avenues)	Classifier training	438 747 846	772 pole-like objects

4. Results and discussion

In this section, the results obtained for the safety assessment of pedestrian crossing environments using MLS data are detailed. These results are compared with manually gathered references, and causes of error together with possible disadvantages of the methodology are discussed. Note that results are offered for every processing module within the methodology presented in Section 2 with the exception of traffic sign classification, as the implemented algorithm relies on previous work whose results have already been discussed in Soilán et al. (2016).

4.1. Accessibility evaluation

The accessibility analysis module outputs qualitative information indicating whether the pedestrian crossing area is part of an accessible pedestrian route. It is given by two binary variables, one for the accessibility of each side of the crossing. A confusion matrix showing the results for the case study presented in Section 3 is presented in Table 2. A total of 54 road entrances were analyzed following the method on Section 2.2 (two entrances for each pedestrian crossing). It can be seen that the entirety of the pedestrian crossings in the case study are accessible. However, there are some cases where the method outputs the opposite. An error analysis shows that the presence of vehicles may lead to the detection of obstacles that are misclassified as curbs, and also to

Table 2
Confusion matrix: Accessibility analysis.

Output/Target	Not Accessible	Accessible
Not Accessible	0	3
Accessible	0	47

occlusions of the crossing area. That is the case for the pedestrian crossing on Fig. 7a. A vehicle, illegally parked on the pedestrian crossing area, causes the algorithm to indicate that the road entrance is not accessible, although there exists a ramp to access the sidewalk.

4.2. Traffic light classification

Traffic lights are classified according to the method on Section 2.3. The metrics used for quantifying the results are Precision, recall, and F-score:

$$Precision = \frac{TP}{TP + FP} \tag{7}$$

$$Recall = \frac{TP}{TP + FN} \tag{8}$$

$$F_{score} = 2 \cdot \frac{Precision \cdot Recall}{Precision + Recall} \tag{9}$$

where TP, FP and FN are, respectively, the number of true positives, false positives and false negatives. Results are shown in Table 3. The classification rates seem promisingly good having in account the simplicity of the features utilized for the classification. Specifically, the classification model for Type 2 traffic lights has been easily trained with a 100% of accuracy, generalizing for the case study data. It is relevant to notice that this classification process includes 5 classes: Traffic Light (Types 1 and 2), street lamp, tree and others. Among the 'others' class, vertical signage have been found to be frequently misclassified as Type 1 street lights. Furthermore, some traffic signs are held on traffic lights, increasing the chance of a false negative. In order to solve this problem, traffic sign panels detected from Section 2.4 algorithm are removed from the pole-like object clusters before the classification process.

4.3. Visibility analysis

Driver-pedestrian visibility analysis is described in Section 2.5. Different points of view, from the stopping distance of the vehicle to the proximity of the pedestrian crossing, are labelled according to the visibility obtained by tracing a line of sight from the driver position to a pedestrian on the sidewalk. The visibility for all 27 pedestrian crossings (therefore, 54 road entrances) of the case study was obtained and qualitative results show that the majority of the points are label indicating good visibility (52 out of 54 analysis). Two of the pedestrian crossing entrances show bad visibility, due to the presence of obstacles close to the pedestrian location, therefore occluding the visibility from the driver point of view (Fig. 7b). Although this analysis is useful in order to locate static, big objects that may occlude the position of a pedestrian, there are several factors that cannot be addressed with the point cloud data. The presence of vehicles double-parked or illegally parked on the pedestrian crossing at the moment of the survey may jeopardize the outputs. Furthermore, the lightning conditions do not have impact on the geometric information gathered by the MMS, hence night-time visibility.

Table 3
Traffic light classification results.

	Precision	Recall	F-score	Number of objects
Traffic Light: Type 1	90.0%	96.4%	93.1%	28
Traffic Light: Type 2	100%	100%	100%	8
Traffic Light: Types 1–2	92.1%	97.2%	94.6%	

5. Conclusions and future work

This work presents an automatic methodology for the assessment of several safety indicators in an urban pedestrian crossing environment, using 3D point cloud data collected with a Mobile Mapping System. The methodology consists in four processing modules, analyzing: Accessibility, presence of traffic lights, presence of traffic signs, and visibility. Each module outputs several parameters that can be exported to a Geographic Information System in order to be visualized. Weighting these parameters according to the criteria of the traffic authorities will allow defining a safety index for each pedestrian crossing, highlighting those areas that need maintenance or any improvement on the geometrical conditions of the crossing area. Conceptually, this work intends to offer an approach towards the automation of infrastructure assessment processes that are conducted manually and subjected to the subjective criteria of the operator. Furthermore, the traffic light classification algorithm presents state-of-the-art results with a global classification score of almost 95%, while using simple, fast to compute features. In essence, a rich semantic description of a specific area within a 3D point cloud is given, with a set of parameters that allow a safety-related definition. This work does not intend to propose a specific safety index, as the criteria for its definition should be agreed with road authorities, but contributes with (1) a framework to extract information from mobile mapping data that allows the eventual definition of a safety index, and (2) proof that mobile mapping is a valid mean for the analysis of certain safety parameters in urban environments.

Future work may have different aspects. On the remote sensing area, there is room for improvement on every processing module that has been developed. The accessibility information should be considered not only for the crossing area but also for the sidewalk. The visibility model can be improved, representing the vision of a driver with more accuracy. Finally, a weighting scheme for the extracted indicators may be needed in order to translate them to a meaningful safety index for a road crossing area.

Fig. 7. Results and error analysis. (a) Occlusions caused by vehicles may lead to a wrong accessibility indicator. (b) Example of a pedestrian crossing with bad visibility; orange points represents points of view labelled as bad visibility, due to the presence of an obstacle.

Acknowledgements

This work has been partially supported by the Dirección General de Tráfico (Spanish Ministry of Interior) (Grant SPIP2017-02122); Xunta de Galicia (Grant ED431C2016-038) and Human Resources program FPI (Grant BES-2014-067736).

References

Abdel-Aty, M., Ekram, A.A., Huang, H., Choi, K., 2011. A study on crashes related to visibility obstruction due to fog and smoke. Accid. Anal. Prev. 43, 1730–1737. http://dx.doi.org/10.1016/j.aap.2011.04.003.

Alsadik, B., Gerke, M., Vosselman, G., 2014. Visibility analysis of point cloud in close range photogrammetry. ISPRS Ann. Photogramm. Remote Sens. Spat. Inf. Sci. II-5 9–16. http://dx.doi.org/10.5194/isprsannals-II-5-9-2014.

Arcos-García, A., Soilán, M., Alvarez-García, J.A., Belén, R., 2017. Exploiting synergies of mobile mapping sensors and deep learning for traffic sign recognition systems. Expert Syst. Appl. 89, 286–295. http://dx.doi.org/10.1016/j.eswa.2017.07.042.

AXA, 2014. Atropellos a peatones 2014. Tráfico y Segur. n°189.

Basile, O., Persia, L., Usami, D.S., 2010. A methodology to assess pedestrian crossing safety. Eur. Trans. Res. Rev. 2, 129–137. http://dx.doi.org/10.1007/s12544-010-0036-z.

Cheng, M., Zhang, H., Wang, C., Li, J., 2017. Extraction and classification of road markings using mobile laser scanning point clouds. IEEE J. Sel. Top. Appl. Earth Obs. Remote Sens. 10, 1182–1196.

Douillard, B., Underwood, J., Kuntz, N., Vlaskine, V., Quadros, A., Morton, P., Frenkel, A., 2011. On the segmentation of 3D lidar point clouds. Proc. IEEE Int. Conf. Robot. Autom. 2798–2805. http://dx.doi.org/10.1109/ICRA.2011.5979818.

ERSO, 2016. Traffic Safety Basic Facts 2016 - Pedestrians. http://dx.doi.org/10.1136/bmj.330.7487.367.

Fundación Mutua Madrileña, 2013. Estudio de siniestralidad vial y atropellos.

González-Jorge, H., Díaz-Vilariño, L., Lorenzo, H., Arias, P., 2016. Evaluation of driver visibility from mobile lidar data and weather conditions. ISPRS - Int. Arch. Photogramm. Remote Sens. Spat. Inf. Sci. XLI-B1, 577–582. http://dx.doi.org/10.5194/isprsarchives-XLI-B1-577-2016.

González-Jorge, H., Riveiro, B., Armesto, J., Arias, P., 2013. Evaluation of road signs using radiometric and geometric data from terrestrial LiDAR. Opt. Appl. 43, 421–433. http://dx.doi.org/10.5277/oa130302.

Guan, H., Li, J., Yu, Y., Wang, C., Chapman, M., Yang, B., 2014. Using mobile laser scanning data for automated extraction of road markings. ISPRS J. Photogramm. Remote Sens. 87, 93–107. http://dx.doi.org/10.1016/j.isprsjprs.2013.11.005.

Hamed, M.M., 2001. Analysis of pedestrians' behavior at pedestrian crossings. Saf. Sci. 38, 63–82. http://dx.doi.org/10.1016/S0925-7535(00)00058-8.

Jiménez-Mejías, E., Martínez-Ruiz, V., Amezcua-Prieto, C., Olmedo-Requena, R., Luna-Del-Castillo, J.D.D., Lardelli-Claret, P., 2016. Pedestrian- and driver-related factors associated with the risk of causing collisions involving pedestrians in Spain. Accid. Anal. Prev. 92, 211–218. http://dx.doi.org/10.1016/j.aap.2016.03.021.

Kelly, C.E., Tight, M.R., Page, M.W., Hodgson, F.C., 2007. Techniques for assessing the walkability of the pedestrian environment. 8th Annu. Int. Conf. Walk. Liveable Communities, Walk 21, 13.

Lassarre, S., Papadimitriou, E., Yannis, G., Golias, J., 2007. Measuring accident risk exposure for pedestrians in different micro-environments. Accid. Anal. Prev. 39, 1226–1238. http://dx.doi.org/10.1016/j.aap.2007.03.009.

Ministerio de Fomento, 2010. Accesibilidad En Los Espacios Públicos Urbanizados. NIPO:751-10-026-3. .

Miyazaki, R., Yamamoto, M., Hanamoto, E., Izumi, H., Harada, K., 2014. A line-based approach for precise extraction of road and curb region from mobile mapping data. ISPRS Ann. Photogramm. Remote Sens. Spat. Inf. Sci. II-5 243–250. http://dx.doi.org/10.5194/isprsannals-II-5-243-2014.

Mueller, A.S., Trick, L.M., 2012. Driving in fog: the effects of driving experience and visibility on speed compensation and hazard avoidance. Accid. Anal. Prev. 48, 472–479. http://dx.doi.org/10.1016/j.aap.2012.03.003.

Puente, I., González-Jorge, H., Martínez-Sánchez, J., Arias, P., 2013a. Review of mobile mapping and surveying technologies. Meas. J. Int. Meas. Confed. 46 (7), 2127–2145. http://dx.doi.org/10.1016/j.measurement.2013.03.006.

Puente, I., González-Jorge, H., Riveiro, B., Arias, P., 2013b. Accuracy verification of the Lynx Mobile mapper system. Opt. Laser Technol. 45, 578–586. http://dx.doi.org/10.1016/j.optlastec.2012.05.029.

RACE, 2009. Informe sobre los pasos de peatones europeos.

RACE; Goodyear, 2015. Informe Race-Goodyear: Atropello de peatones en zona urbana.

Retting, R.A., Ferguson, S.A., McCartt, A.T., 2003. A review of evidence-based traffic engineering measures designed to reduce pedestrian-motor vehicle crashes. Am. J. Public Health 93, 1456–1463. http://dx.doi.org/10.2105/AJPH.93.9.1456.

Riveiro, B., Diaz-Vilarino, L., Conde-Carnero, B., Soilan, M., Arias, P., 2015. Automatic segmentation and shape-based classification of retro-reflective traffic signs from Mobile LiDAR data. IEEE J. Sel. Top. Appl. Earth Obs. Remote Sens. 9 (1), 295–303. http://dx.doi.org/10.1109/JSTARS.2015.2461680.

Serna, A., Marcotegui, B., 2014. Detection, segmentation and classification of 3D urban objects using mathematical morphology and supervised learning. ISPRS J. Photogramm. Remote Sens. 93, 243–255. http://dx.doi.org/10.1016/j.isprsjprs.2014.03.015.

Serna, A., Marcotegui, B., 2013. Urban accessibility diagnosis from mobile laser scanning data. ISPRS J. Photogramm. Remote Sens. 84, 23–32. http://dx.doi.org/10.1016/j.isprsjprs.2013.07.001.

Soilán, M., Riveiro, B., Martínez-Sánchez, J., Arias, P., 2017. Segmentation and classification of road markings using MLS data. ISPRS J. Photogramm. Remote Sens. 123, 94–103. http://dx.doi.org/10.1016/j.isprsjprs.2016.11.011.

Soilán, M., Riveiro, B., Martínez-Sánchez, J., Arias, P., 2016. Traffic sign detection in MLS acquired point clouds for geometric and image-based semantic inventory. ISPRS J. Photogramm. Remote Sens. 114, 92–101. http://dx.doi.org/10.1016/j.isprsjprs.2016.01.019.

US Department of Transportation, 2001. Pedestrian Facilities Users Guide. Providing Safety and Mobility.

Várhelyi, A., 1998. Drivers' speed behaviour at a zebra crossing: A case study. Accid. Anal. Prev. 30, 731–743. http://dx.doi.org/10.1016/S0001-4575(98)00026-8.

Wang, H., Luo, H., Wen, C., Cheng, J., Li, P., Chen, Y., Wang, C., Li, J., 2015. Road boundaries detection based on local normal saliency from Mobile laser scanning data. IEEE GeoSci. Remote Sens. Lett. 12, 2085–2089.

Wen, C., Li, J., Member, S., Luo, H., Yu, Y., Cai, Z., Wang, H., Wang, C., 2015. Spatial-related traffic sign inspection for inventory purposes using Mobile laser scanning data. IEEE Trans. Intell. Trans. Syst. 17, 27–37. http://dx.doi.org/10.1109/TITS.2015.2418214.

Yang, B., Dong, Z., Liu, Y., Liang, F., Wang, Y., 2017. Computing multiple aggregation levels and contextual features for road facilities recognition using mobile laser scanning data. ISPRS J. Photogramm. Remote Sens. 126, 180–194. http://dx.doi.org/10.1016/j.isprsjprs.2017.02.014.

Yang, B., Dong, Z., Zhao, G., Dai, W., 2015. Hierarchical extraction of urban objects from mobile laser scanning data. ISPRS J. Photogramm. Remote Sens. 99, 45–57. http://dx.doi.org/10.1016/j.isprsjprs.2014.10.005.

Yu, Y., Li, J., Guan, H., Jia, F., Wang, C., 2015a. Learning hierarchical features for automated extraction of road markings from 3-D Mobile LiDAR point clouds. IEEE J. Sel. Top. Appl. Earth Obs. Remote Sens. 8, 709–726.

Yu, Y., Li, J., Guan, H., Wang, C., Yu, J., 2015b. Semiautomated extraction of Street light poles from Mobile LiDAR point-clouds. IEEE Trans. Geosci. Remote Sens. 53, 1374–1386. http://dx.doi.org/10.1109/TGRS.2014.2338915.

Yu, Y., Li, J., Wen, C., Guan, H., Luo, H., Wang, C., 2016. Bag-of-visual-phrases and hierarchical deep models for traffic sign detection and recognition in mobile laser scanning data. ISPRS J. Photogramm. Remote Sens. 113, 106–123. http://dx.doi.org/10.1016/j.isprsjprs.2016.01.005.

Zhou, L., Vosselman, G., 2012. Mapping curbstones in airborne and mobile laser scanning data. Int. J. Appl. Earth Obs. Geoinf. 18, 293–304. http://dx.doi.org/10.1016/j.jag.2012.01.024.